Environmental Research 199 (2021) 111360

Contents lists available at ScienceDirect

Environmental Research

journal homepage: www.elsevier.com/locate/envres

A review of bismuth-based photocatalysts for antibiotic degradation: Insight into the photocatalytic degradation performance, pathways and relevant mechanisms

Kena Qin [a], Qingliang Zhao [a], Hang Yu [a], Xinhui Xia [a], Jianju Li [a], Shufei He [a], Liangliang Wei [a,**], Taicheng An [b,*]

[a] State Key Laboratory of Urban Water Resources and Environment (SKLUWRE), School of Environment, Harbin Institute of Technology, Harbin, 150090, China
[b] Guangzhou Key Laboratory of Environmental Catalysis and Pollution Control, Key Laboratory of City Cluster Environmental Safety and Green Development, School of Environmental Science and Engineering, Guangdong University of Technology, Guangzhou, 510006, China

ARTICLE INFO

Keywords:
Bismuth-based photocatalysts
Antibiotics
Photocatalytic degradation
Performance
Mechanism

ABSTRACT

The intensive production and utilization of antibiotics worldwide has inevitably led to releases of very large amounts of these medicines into the environment, and numerous strategies have recently been developed to eliminate antibiotic pollution. Therefore, bismuth-based photocatalysts have attracted much attention due to their high adsorption of visible light and low production cost. This review summarizes the performance, degradation pathways and relevant mechanisms of typical antibiotics during bismuth-based photocatalytic degradation. First, the band gap and redox ability of the bismuth-based catalysts and modified materials (such as morphology, structure mediation, heterojunction construction and element doping) were compared and evaluated. Second, the performance and potential mechanisms of bismuth oxides, bismuth sulfides, bismuth oxyhalides and bismuth-based metal oxides for antibiotic removal were investigated. Third, we analysed the effect of co-existing interfering substances in a real water matrix on the photocatalytic ability, as well as the coupling processes for degradation enhancement. In the last section, current difficulties and future perspectives on photocatalytic degradation for antibiotic elimination by bismuth-based catalysts are summarized. Generally, modified bismuth-based compounds showed better performance than single-component photocatalysts during photocatalytic degradation for most antibiotics, in which h^+ played a predominant role among all the related reactive oxygen species. Moreover, the crystal structures and morphologies of bismuth-based catalysts seriously affected their practical efficiencies.

1. Introduction

Antibiotics have been acclaimed as one of the major achievements in the history of microbiology because of their excellent therapeutic effects on bacterial infections. In recent years, people have increasingly depended on antibiotics and have used them excessively. Statistically, global antibiotic consumption was 35 billion defined daily doses in 2015 (Antoñanzas and Goossens, 2019). Unfortunately, those consumed antibiotics cannot be completely metabolized in the human body or animals and are partially excreted through faeces and urine. Consequently, parent compounds and their metabolites are widely present in municipal wastewater, surface water and groundwater. It was estimated that a total of 53,800 tons of antibiotics were released to rivers and waterways in China in 2013 (Zhang et al., 2015). Although antibiotics usually have a shorter half-life than persistent organic materials (Trojanowicz, 2020), the sustained use of antibiotics has resulted in incessant exposure in the environment, rendering them pseudo-persistent (Patel et al., 2019).

There is growing concern that residual antibiotics in aquatic ecosystems may cause a risk to human health. First, long-term antibiotic exposure may affect the distribution of the microbial community in the aqueous matrix and subsequently affect other advanced living organisms through food chain transmission, endangering the safety of the ecosystem (Meredith et al., 2015). Second, the prevalence of antibiotics at a low concentration may promote the selection of antibiotic resistance

* Corresponding author.
** Corresponding author.
E-mail addresses: weill333@163.com (L. Wei), antc99@gdut.edu.cn (T. An).

https://doi.org/10.1016/j.envres.2021.111360
Received 20 March 2021; Received in revised form 6 May 2021; Accepted 17 May 2021
Available online 19 May 2021

genes (ARGs) and antibiotic-resistant bacteria (ARB) (Berendonk et al., 2015; Qin et al., 2020a, 2020b). Third, antibiotic residues have caused great risks of acute and chronic toxicity and serious harm to human health. For example, the accumulation of tetracycline can inhibit bone growth in children (Daghrir and Drogui, 2013); sulfonamides can easily cause allergies in sensitive individuals (Giles et al., 2019). Therefore, it is imperative to develop valid technology to thoroughly eliminate antibiotics from water, and various strategies have been employed to solve the problem of antibiotic pollution in recently (Xia et al., 2021).

Biotic elimination processes, such as biodegradation by bacteria and fungi, and non-biotic processes, including sorption, hydrolysis, electrolysis, oxidation, and reduction, have attracted much attention (Cheng and Hu, 2017; Y. Liu et al., 2017; Qin et al., 2020a, 2020b; Wei et al., 2017). Specifically, the photocatalytic degradation of antibiotics based on semiconductors is an effective, eco-friendly and promising method for toxic antibiotic degradation (Ajiboye et al., 2021). These antibiotics are finally deconstructed into small molecules or mineralized into CO_2 and H_2O by oxidative radicals generated from semiconductor photoexcitation even under mild operation conditions (Sturini et al., 2012). In recent years, many researchers have been devoted to fabricating new photocatalysts to eliminate antibiotics with satisfactory efficiency (Wang et al., 2020; An et al., 2015). For example, Zhu et al. (2013) used nanosized TiO_2 to degrade tetracycline in water under UV irradiation, and 95% of tetracycline (20 mg/L) was eliminated after 60 min. However, TiO_2 can be excited only by ultraviolet light with wavelengths shorter than 387.5 nm (approximately only 4% of the solar light spectrum). Thus, to better exploit the solar light spectrum, it is highly desirable to develop and synthesize advanced photocatalyst systems with enhanced photocatalytic activities that can also be activated by visible-light irradiation. Recently, g-C_3N_4, silver, and bismuth-based catalysts have been hot areas of research due to their narrow band gap and strong absorption in the visible light region (Chen et al., 2017; B. Li et al., 2018; Nabi et al., 2019). Song et al. (2020) found that ZnO/$AgVO_3$ composites with an optimal $AgVO_3$ content could remove 90% of ciprofloxacin (10 mg/L) after 90 min of reaction. Similarly, 91.2% tetracycline (10 mg/L) could be effectively decreased via the photocatalytic degradation of Ag_3PO_4/$Co_3(PO_4)_2$@Ag in 60 min (Shi et al., 2020)and 100% levofloxacin (20 mg/L) by Cu_2-xS/g-C_3N_4 in 20 min irradiation with simulated sunlight (Zhou et al., 2020). However, photogenerated electrons will reduce Ag^+ to Ag nanoparticles for silver-based catalysts and cause photo-corrosion (Dai et al., 2012). For g-C_3N_4, the inherent disadvantage is the rapid recombination of photogenerated electrons and holes, as well as their relatively small specific surface area (Yin et al., 2015).

In comparison with the aforementioned visible light catalysts, bismuth-based photocatalysts have the following advantages: low production cost, high photostability, narrow band gap, resistance to photocorrosion, large specific area/pore volume and so on (Malathi et al., 2018). Numerous recent reviews have focused on the development of bismuth-based composite oxides for photocatalytic hydrogen generation (Fang and Shangguan, 2019), water oxidation (Huang et al., 2014) and dye degradation (Ponraj et al., 2017; Singh et al., 2018; Sivakumar et al., 2014). However, there is a paucity of collective information on the applications of bismuth-based photocatalysts in antibiotic degradation. For the purpose of enhancing the degradation of antibiotics via the construction of novel bismuth-based photocatalysts with high efficiency and low cost, the design and synthesis of different bismuth-based photocatalysts for the photocatalytic degradation of antibiotics were summarized first. Then, the performance, degradation pathways of typical antibiotics, and potential mechanisms during bismuth-based catalyst degradation were evaluated. Third, the challenges and future perspectives of the application of those bismuth-based catalysts were emphatically analysed.

2. Classification, band gaps of typical bismuth-based photocatalysts and the dominant photocatalytic degradation mechanisms for antibiotic removal

2.1. Classification of bismuth-based photocatalysts and band gap distribution

Bismuth, with an atomic electron configuration of $6s^26p^3$, is a metallic element from the fifth group of the sixth period in the periodic table and usually exists in the form of Bi^{3+} (Zhang et al., 2018). The lone-pair distortion of the Bi 6s orbital in bismuth-based complex oxides may lead to the overlap of O 2p and Bi 6s orbitals in the valence band, which benefits the reduction of the band gap and mobility of photoinduced charges, as well as improving the visible light response performance. Meanwhile, the Bi^{5+} valence state also has good absorption of visible light once the 6s orbital is empty (Liu et al., 2017). Recently, a series of new bismuth-based photocatalysts with different crystal structures have been reported, and they can generally be classified as bismuth oxides, sulfides, oxyhalides and metal oxides according to their composition. The corresponding band gaps of typical bismuth-based photocatalysts are listed in Table 1.

Most bismuth-based catalysts, listed in Table 1, are active under visible light irradiation, with a band gap of less than 3.0 eV, except for $Bi_5FeTi_3O_{15}$, BiOF, δ-Bi_2O_3, and BiOCl. Specifically, the band gaps of Bi_2S_3, BiOI and $LiBiO_3$ are <2.0 eV, implying their excellent performance in visible light adsorption. To enhance the mineralization rate of residual antibiotics in wastewater, a high charge-separation efficiency, long-term stability, appropriate band edge positions and strong redox ability were also needed for the photocatalysts in addition to a narrow band gap (Zhou et al., 2014). Thus, numerous controllable bismuth-based compounds have been prepared via morphology/-structure mediation, heterojunction construction and element doping because single-component photocatalysts cannot achieve such characteristics simultaneously (Ding et al., 2017). The characteristics of different bismuth-based catalysts and their performance in antibiotic photocatalytic degradation are described in detail in the following sections.

2.2. Fundamental mechanism and main active species of typical bismuth-based photocatalysts for antibiotic degradation

The predominant mechanisms of the bismuth-based photocatalysts for antibiotic photocatalytic degradation could be summarized as absorbing photons, excitation and reaction (Fig. 1). Specifically, once the photocatalyst absorbs photons with energy higher than its band gap, the electrons in the valence band could be excited and jump into the conduction band ((1)Eq. (1)); thereafter, the photoinduced electrons and holes were efficiently separated and migrated to the surface of the photocatalyst. Photogenerated holes attacked those antibiotics directly (Eq. (2)) and theoretically led to a significant degradation of those toxic antibiotics. In addition, the oxidative pathway was initiated when the holes further migrated to the photocatalyst surface, accompanied by hydroxyl radical (•OH) generation upon the oxidation of H_2O/OH^- (Eq. (3)). In this case, the standard redox potential of photocatalysts should be higher than that of $•OH/OH^-$ (+1.99 eV) (Yang et al., 2018). In fact, hydroxyl radicals have stronger oxidation potentials ($E^0 = 2.8$ eV) and lower selection than other oxidants during the decomposition of aqueous contaminants (Homem and Santos, 2011; Lee and von Gunten, 2012). Interestingly, almost all the tops of the valence band bismuth-based photocatalysts are higher than the redox potential of $•OH/OH^-$ (+1.99 eV) (Fig. 2), implying that hydroxyl radicals can be easily generated during bismuth-based catalysing. Generally, the reaction pathway between the hydroxyl radical and antibiotics could be summarized as follows: (1) both •OH and antibiotics are simultaneously adsorbed on the surface of the catalyst and then react; (2) •OH in the solution reacts with the antibiotics adsorbed on the surface of the

Table 1
A summary of the typical bismuth-based photocatalysts and the detailed information of their band gaps, crystal structures and etc.

Categories	General formula	Compounds	Band gap (ev)	Crystal structure	References
Bi_2X_3	Bi_2O_3	γ-Bi_2O_3	1.64	body-centered cubic	Gurunathan (2004)
		α-Bi_2O_3	2.8–2.91	monoclinic	(Ho et al., 2013; Wu et al., 2020; Yan et al., 2014a)
		β-Bi_2O_3	2.1–2.4	tetragonal	(Li et al., 2018; Schlesinger et al., 2013; Yan et al., 2014b)
		δ-Bi_2O_3	3.01–3.55	cubic fluorite-type	Xie et al. (2012)
	Bi_2S_3	Bi_2S_3	1.3	orthorhombic	Shahbazi et al. (2020a)
Binary compounds	BiOX	BiOF	3.6	–	Su et al. (2010)
		BiOCl	3.5	tetragonal	Wang et al. (2007)
		BiOBr	2.6	tetragonal	Ye et al. (2014)
		BiOI	1.8–1.9	tetragonal	Ye et al. (2014)
Multi-component bismuth compounds	$Bi_xM_yO_z$	$Bi_2Ti_2O_7$ $Bi_4Ti_3O_{12}$ $Bi_{12}TiO_{20}$ $Bi_2Ti_4O_{11}$ $Bi_{20}Ti_2O_{32}$	2.5–2.7	–	(Murugesan et al., 2010); (Nogueira et al., 2014)
		Bi_2WO_6	2.77–2.8	orthorhombic	(Shahbazi et al., 2020b); Yu et al. (2005)
		$BiVO_4$	2.3–2.5	monoclinic; tetragonal; octahedral	Ajiboye et al. (2021)
		Bi_2MO_6	2.63	–	Bi et al. (2007)
		Bi_2MoO_6	2.7	orthorhombic	Lou et al. (2018)
	$M_yBi_xO_z$	Bi_2CrO_6	1.99	–	Li et al. (2020)
		$KBiO_3$	2.04	–	Zheng et al. (2018)
		$NaBiO_3$	2.2	–	Liu et al. (2013)
		$LiBiO_3$	1.8	–	Ramachandran et al. (2011)
		$AgBiO_3$	0.8–2.5	–	Boruah et al. (2019)
	Others	$Bi_5FeTi_3O_{15}$	3.2	–	Zuo et al. (2019)

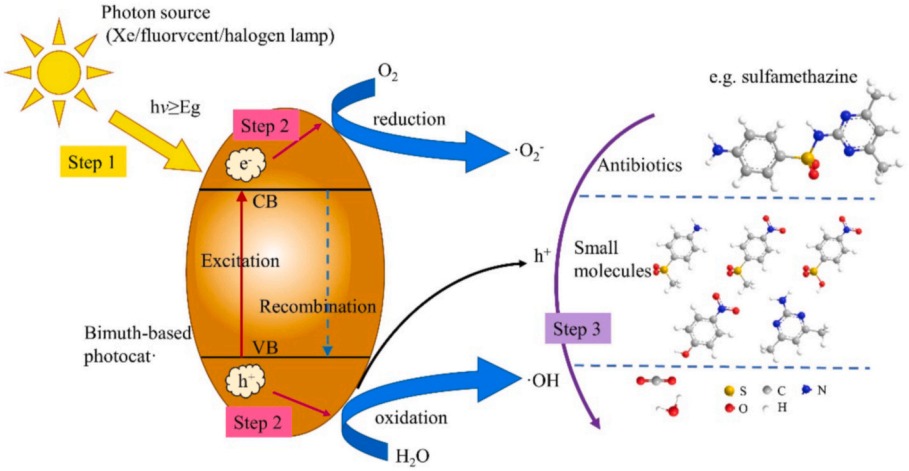

Fig. 1. Degradation mechanisms of antibiotics by bismuth-based photocatalysts.

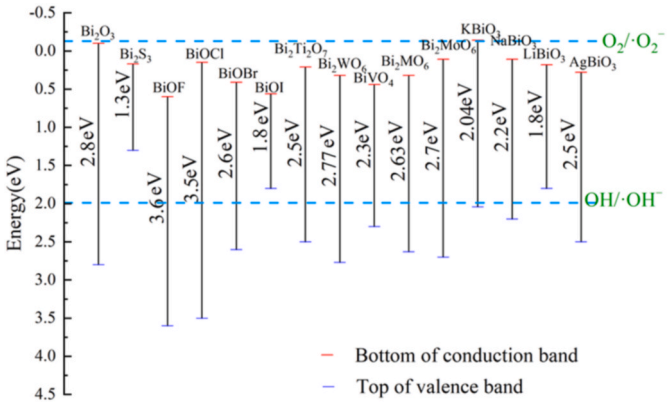

Fig. 2. The band edge positions of bismuth-based photocatalysts.

catalyst; (3) •OH adsorbed on the surface of the catalyst reacts with the surrounding antibiotics; and (4) •OH reacts with antibiotics in solution. Specifically, the first pathway has been regarded as the dominant pathway for antibiotic photocatalytic degradation by bismuth-based catalysts (Guo et al., 2017; Chen et al., 2020).

In contrast, a reductive pathway could also be observed if the conduction band potential of the semiconductor is negative compared to that of the $O_2/\bullet O_2^-$ redox potential (−0.13 eV versus normal hydrogen electrode (NHE)), wherein O_2 is reduced by electrons to $\bullet O_2^-$ (Eq. (4)) (Kaur and Kansal, 2016). After being excited, hydrogen ions could recombine with the electrons and generate heat energy (Eq. (5)), which would decrease the efficiency of the photodegradation.

Then, the antibiotics, as well as their intermediates, were converted to small molecule compounds via the oxidation of oxygen species (h^+, $\bullet O_2^-$ or •OH) and eventually decomposed into CO_2 and H_2O (Eq. (6)).

$$\text{Photocatalyst} + h\nu \rightarrow \text{photocatalyst} + h^+ + e^- \quad (1)$$

$$h^+ + \text{antibiotics} \rightarrow H_2O + CO_2 + \text{degradation products} \quad (2)$$

$$H_2O/OH^- + h^+ \rightarrow \bullet OH + H^+ \quad (3)$$

$$O_2 + e^- \rightarrow \bullet O_2^- \quad (4)$$

$$H^+ + e^- \rightarrow \text{energy} \quad (5)$$

$$\text{Antibiotics} + \text{radicals } (\bullet OH \text{ or } \bullet O_2^-) \rightarrow CO_2 + H_2O + \text{small molecule compounds} \quad (6)$$

However, the roles of diverse active species vary for degradation of different antibiotics due to their dissimilar electronic structures. To detect the priority active species during the reaction, various scavengers, such as KI (scavenger for h^+), $AgNO_3$ (scavenger for e^-), MeOH (scavenger for •OH), and benzoquinone (scavenger for $\bullet O_2^-$), were added into the reactors to trap the active species (Zhao et al., 2021), and detailed information can be found in Table 2. Clearly, h^+ played the predominant role during the photocatalytic degradation of bismuth-based photocatalysts for most antibiotics (Zhang et al., 2015; Zhu et al., 2020). Taking quinolones as an example, the main reason for their higher photocatalytic degradation might be that the piperazine moiety was considered vulnerable to h^+ attack (Lv et al., 2020; Zhang et al., 2015; An et al., 2010a, 2010b). Moreover, the oxazole ring of sulfonamides can also be attacked by h^+ (Ling et al., 2020). In addition, hydroxyl radicals (•OH) usually react rapidly and non-selectively with most organic contaminants; thus, they also play a critical role in antibiotic photocatalytic degradation (Table 2). As shown in Table 2, the generated $\bullet O_2^-$ in is unstable, and disproportionation easily occurs to produce other ROS (reaction oxygen species) including •OH (Zhang et al., 2010).

2.3. Bond breakage of antibiotics during typical bismuth-based photocatalytic degradation

Destruction of the chemical structures and bond breakage information of typical antibiotics (sulfonamides, quinolones, tetracyclines, cephalosporins, etc.) during typical bismuth-based photocatalytic degradation are summarized, and the results are listed in Fig. 3. Taking sulfamethoxazole (SMZ) as an example (Fig. 3a), the S–N bond was considered a very vulnerable bond to be attacked by $\bullet O_2^-$ (marked as pathway 1), and the oxazole ring can be easily destroyed via ROS attack (marked as pathway 2). Meanwhile, hydroxylation of the benzene ring and the connected NH_2^- have also been widely reported (pathways 3 and 4) (Niu et al., 2013). Overall, intermediate products of antibiotics are produced under a series of hydration, replacement and oxidative processes with the attack of reaction oxygen species (ROS), and ring structures can be further oxidized and ruptured.

Although the majority of antibiotics were efficiently destroyed by the active species generated from bismuth-based compounds, some researchers also persisted that those antibiotics could not be thoroughly mineralized (An et al., 2010a, 2010b) and eventually converted into metabolites or intermediates. For instance, Chu et al. (2016) revealed that only 31% of the total organic carbon (TOC) was removed after 360 min of irradiation with Bi_2WO_6 (0.5 g L^{-1}), although a removal rate as high as 100% of tetracycline (TC) was observed. Since those antibiotics, as well as their metabolites, intermediates, or precursors, can significantly affect the bacteriostatic activity in wastewater, further work is needed to enhance bulk oxidation.

3. Efficiencies, characteristics and operational parameters of bismuth-based compounds for antibiotic photocatalytic degradation

3.1. Performance of bismuth oxides

Bismuth oxide, a common oxide semiconductor, has been reported to have various crystal structures, including γ-Bi_2O_3 (body-centered cubic), β-Bi_2O_3 (tetragonal), δ-Bi_2O_3 (cubic fluorite type) and α-Bi_2O_3 (monoclinic). The order of the band gap of these four structures is γ-Bi_2O_3 (1.64 eV) <β-Bi_2O_3 (2.1 eV) < α-Bi_2O_3 (2.8 eV) < δ-Bi_2O_3 (3.0 eV) (Gurunathan, 2004). Specifically, α-Bi_2O_3 is the only stable phase over a wide temperature range, while β-, δ-, and γ-Bi_2O_3 are metastable at room temperature. Clearly, γ-Bi_2O_3 has the narrowest band gap; thus, it can efficiently utilize light in the visible region of the solar spectrum (Wang et al., 2017). However, the photocatalytic efficiency of pure Bi_2O_3 is still insufficient for antibiotics unless it is doped with suitable compounds, especially for the δ-phase (which exhibited the highest band gap among all phases of Bi_2O_3). For this purpose, several approaches have been applied for enhancing the photocatalytic activity of Bi_2O_3, such as heterostructure construction, cation/anion/zerovalent element doping, and shrinkage of the Bi_2O_3 band gap. The latest investigations on modified Bi_2O_3 for antibiotic degradation are summarized, and detailed information can be found in Table 3. Wu et al. (2020) prepared Bi-bridged Z-scheme BiOCl/Bi_2O_3 heterojunctions with oxygen vacancies via a one-step hydrothermal method and proved that it exhibited excellent photocatalytic activity in degrading TC (with a removal efficiency of 94.79%) due to the enhanced separation of the photogenerated electron–hole pairs and the high redox ability of the Z-scheme. Ren et al. (2014) demonstrated that 50% $NiFe_2O_4$/Bi_2O_3 heterostructures exhibit effective electron hole pair separation and achieved a TC degradation of 90.78% in 90 min (only 70% for Bi_2O_3). Moreover, the heterostructures can be recovered under a magnetic field similar to the magnetic core–shell Fe_3O_4@Bi_2O_3–RGO heterojunctions (Zhu et al., 2017). In addition to the efficient separation of photogenerated electron–hole pairs, the photocatalytic properties of semiconductors are highly dependent on

Table 2
The main active species of different bismuth-based photocatalysts for antibiotic degradation.

Class	Antibiotic	Radicals (rank by obviousness)	Bismuth-based photocatalyst	Band gap	Reference
Quinolones	ciprofloxacin	$\bullet O_2^- > h^+ > \bullet OH$	Z-scheme Ag/AgBr/$BiVO_4$	–	Chen et al. (2018)
	levofloxacin	$e^- > \bullet OH > h^+ > \bullet O_2^-$,	Bi_2WO_6 nanocuboids	2.61	Kaur and Kansal (2016)
	ciprofloxacin	h^+	BiOBr	2.55	Zhang et al. (2015)
	norfloxacin	$h^+ > \bullet OH > \bullet O_2^-$	Ag_3PO_4/Bi_2WO_6/Multi-Walled Carbon Nanotubes	2.75	Zhu et al. (2020)
Tetracyclines	tetracycline	•OH, $\bullet O_2^-$	$BiVO_4$/TiO_2/RGO	2.29	Wang et al. (2019)
	doxycycline	•OH, $\bullet O_2^-$	$BiVO_4$/TiO_2/RGO	2.29	Wang et al. (2019)
	tetracycline hydrochloride	$h^+ > \bullet O_2^- > \bullet OH$	g-C_3N_4/BiOBr	–	Shi et al., 2020
	tetracycline	$h^+ > \bullet OH$	monoclinic–tetragonal $BiVO_4$	2.3	Ming et al. (2015)
Sulfonamides	sulfamethazine	$\bullet O_2^-$, h^+	Bi_2O_3–TiO_2/PAC Ternary Nanoparticles	–	Zhuang et al. (2020)
	sulfamethazine	$h^+ > \bullet O_2^- > \cdot OH$	m-Bi_2O_4	2.08	Chen et al. (2019)
	sulfamethazine	$h^+ > \bullet O_2^- > \cdot OH$	Z-Scheme AgI/$Bi_4V_2O_{11}$ photocatalyst	–	Wen et al. (2020)
	sulfamethoxazole	$\bullet O_2^- > h^+$	TiO_2 nanocrystals in situ wrapped-Bi_2O_4microrods	2.015	Ling et al. (2020)
	sulfamethoxazole	$\bullet OH > \bullet O_2^-$	BiOCl/g-C_3N_4/Cu_2O/Fe_3O_4 nano-junction	2.58	Kumar et al. (2018)
Cephalosporins	ceftriaxone sodium	$h^+ > \bullet O_2^- > \bullet OH$	Bi_2WO_6/g-C_3N_4	–	Zhao et al. (2018)

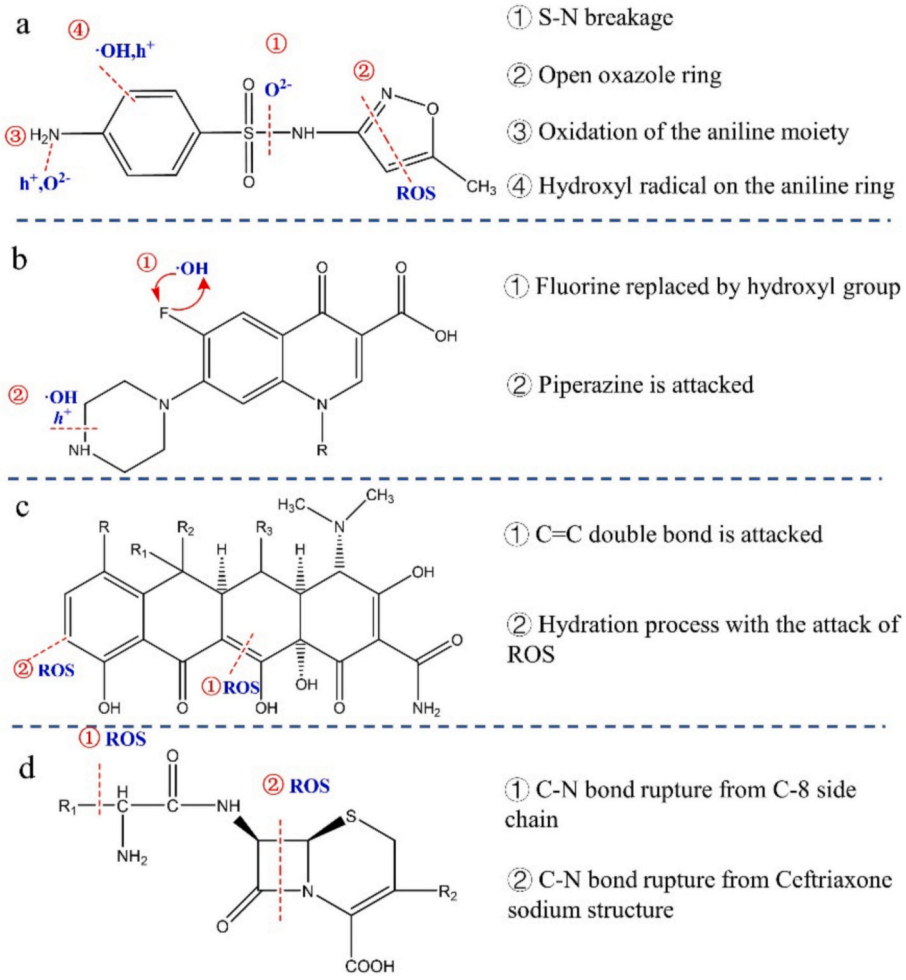

Fig. 3. Structural destruction and bond breakage of typical antibiotics (a. sulfonamides; b. quinolones; c. tetracyclines; d. cephalosporins) during typical bismuth-based catalyst photocatalytic degradation.

Table 3
Comparison of the catalytic activity of bismuth-oxides for antibiotic degradation.

Photocatalyst	Dosage	Light source	Antibiotics	Concentration/volume of antibiotics	Preparation methods	Irradiation time/ degradation efficiency	References
Bi_2O_3 nanotubes	0.1 g	300 W Xe	tetracycline	10 mg L^{-1}/100 mL	microwave-assisted synthetic method	1 h/80%	Zhang et al. (2013)
50%$NiFe_2O_4$/**Bi_2O_3** heterostructures	0.1 g	150 W Xe	tetracycline	10 mg L^{-1}/100 mL	microwave-assisted synthetic method	90 min/90.78%	Ren et al. (2014)
magnetic core–shell Fe_3O_4@**Bi_2O_3**–RGO heterojunctions	0.01 g	500 W Xe	ciprofloxacin	20 mg L^{-1}/40 mL	a self-assembly method	240 min/98.3%	Zhu et al. (2017)
Z-scheme BiOCl/Bi–**Bi_2O_3** heterojunction	0.02 g	300 W Xe	tetracycline	10 mg L^{-1}/100 mL	hydrothermal method	150 min/94.79%	Wu et al. (2020)
Phosphate-modified m-**Bi_2O_4**	0.02 g	350 W Xe	sulfamethazine	8 mg L^{-1}/50 mL	hydrothermal method	60 min/ > 95%	Chen et al. (2020)
$BiOCl_{0.9}I_{0.1}$/β-**Bi_2O_3** composite	–	350 W Xe	tetracycline	20 mg L^{-1}/50 mL	precipitation method	120 min/82.4%	Ma et al. (2020)

their morphologies and sizes.

To date, Bi_2O_3 has been reported to have various morphologies, including nanoparticles, nanorods, nanowires, nanofibres and thin films (Zhao et al., 2004; Vila et al., 2013; Wu et al., 2011), which can modify the active specific surface of catalysts and significantly enhance antibiotic removal (Reverberi et al., 2018). Zhang et al. (2013) synthesized monoclinic Bi_2O_3 nanotubes via a rapid microwave-assisted synthetic method, and 83.63% of tetracycline was photodegraded under visible light in 60 min. However, only 72% of tetracycline was degraded under day-long exposure to radiation from a xenon lamp with Bi_2O_3 nanoplates (Sánchez-Martínez et al., 2016).

3.2. Performance of bismuth sulfides

Bi_2S_3 exhibits an orthorhombic crystal structure and a band gap energy of 1.30 eV, molecular weight of 514.1 g mol^{-1}, density of 6.8 g cm^{-3} and melting point of 775 °C (Mohammad-AliShahbazi et al., 2020). These properties guaranteed its potential application as a

visible-light photocatalyst. However, the narrow band gap between the conduction band and its valence band implies a facile recombination of photogenerated electrons and holes. In addition, the serious photo-corrosion of Bi_2S_3 further restricts its photocatalytic activity. Therefore, few studies have employed pure Bi_2S_3 to photodegrade antibiotics. Recently, some modified photocatalysts with high availability of visible light and good inhibition of electronic-hole recombination have been synthesized, and the detailed information is summarized in Table 4. Askari et al. (2020) used a ternary heterojunction of double Z-scheme $CuWO_4/Bi_2S_3$/ZIF67 to degrade metronidazole (MTZ) and cephalexin (CFX) under LED (400 W/m^2, $\lambda > 400$ nm) illumination, leading to maximum degradation efficiencies of 95.6% for MTZ and 90.1% for CFX, approximately 9 times higher than that of Bi_2S_3. Similarly, Z-scheme $LaTiO_2N/Bi_2S_3$@RGO(LBR) nano-heterostructures were prepared by a solvothermal method and showed remarkable performance in TC photodegradation under visible light irradiation, and 96.4% of TC was eliminated within 90 min under visible light. TC degradation with the LBR heterojunction was also ~9 times faster than that with bare Bi_2S_3 (Sharma et al., 2020). Compared with binary composites, ternary conjunctions of Bi_2S_3 can separate charges and increase visible light absorption, resulting in remarkable enhancement in photocatalytic activity (Wu and Xing, 2018). Under almost the same conditions, the catalytic efficiency of Bi_2S_3-pillared g-C_3N_4 is inferior to that of $LaTiO_2N/Bi_2S_3$ Z-scheme nano-heterostructures, which require a longer time (150 min) to reach the same level removal efficiency (92.5%) (Chen et al., 2017). Overall, it is difficult to simultaneously achieve efficient charge carrier separation and high redox ability in conventional heterojunctions. The enhancement in photocatalytic activity is primarily attributed to Z-scheme charge transfer between $LaTiO_2N$ and Bi_2S_3, which is facilitated by reduced graphene oxide sheets via strong interfacial contact maintaining high potential for redox conversions (Bao et al., 2018). It is interesting that increasing the operational temperatures benefited the adsorption of the antibiotics on the active surface of the catalyst, decreased the aggregation of pollutant particles, and improved the electron-hole pair generation. However, a further increase in temperature results in more recombination of photoinduced charge carriers, as well as a decline in dissolved oxygen. Moreover, the weight ratios of Bi_2S_3 specifically affect the photocatalytic activity of the heterojunction, which has been recently emphasized (Chen et al., 2017).

3.3. Performance of bismuth oxyhalides

Binary bismuth-based catalysts usually contain bismuth-oxyhalide and bismuth-based metal oxides. Bismuth oxyhalides have been proven to exhibit remarkable photocatalytic activity owing to their unique layered structures, which can induce the effective separation of photogenerated electron–hole pairs. The band gap of bismuth-oxyhalides decreases with an increase in the halogen atomic number (BiOF 3.6 eV > BiOCl 3.5 eV > BiOBr 2.6 eV > BiOI 1.8–1.9 eV). BiOCl, a p-type semiconductor with a band gap of 3.5 eV, can only absorb UV light (Zhang et al., 2015). However, this material shows much higher photo-corrosion stability than visible light-absorbing BiOBr and BiOI. BiOI microspheres have been successfully applied to degrade TC under visible light, and 94% of TC was removed after 120 min of operation, whereas the corresponding removal rate of TOC was only 28.68% (Hao et al., 2012). The results indicated that TC was mainly transformed to intermediate products but not completely mineralized. Most BiOI catalysts with three-dimensional (3D) or porous structures were traditionally synthesized in complicated solvent systems under high temperature/pressure for long reaction periods. This was the main barrier for the practical application of BiOI. Among bismuth oxyhalides, BiOBr has been recognized as the best visible-light photocatalyst for antibiotic degradation (Huo et al., 2012). For example, Zhang et al. (2015) synthesized flake-shaped BiOBr via a hydrothermal method, and ciprofloxacin (with an initial concentration of 5 mg/L) was degraded completely within 140 min under visible light irradiation. Intriguingly, CIP (ciprofloxacin) oxidation is dominated by the direct hole oxidation process during the visible light-induced photocatalytic process on BiOBr, whereas •OH (the common active species in advanced oxidation processes) is not effective. It was also noted that the mineralization of CIP was incomplete and closely related to the resistance of the core quinolone ring.

To overcome these barriers, enormous effort has been made to maximize antibiotic abatement, such as developing heterojunctions or doping with metals. Generally, doping with metal/nonmetal ions can introduce an intermediate energy level for the purpose of narrowing the energy band. Moreover, Lv et al. (2020) found that the introduction of Cu into BiOBr could enhance the adsorption capacity between the photocatalyst and norfloxacin, which is considered to be the main reason for efficiency improvement. After 90 min, 99% of norfloxacin was removed under the application of copper-doped BiOBr microflowers, which is 2.28 times higher than that of undoped BiOBr. The other photocatalytic performances of BiOX heterojunctions are shown in Table 5. Obviously, the removal efficiency for different antibiotics is more than 80% within 120 min. In addition, density functional theory (DFT) calculations show that the valence band (VB) of BiOBr is composed of hybrid Br 4p, O 2p and Bi 6s orbitals, whereas the conduction band (CB) bottom primarily consists of Bi 6p orbitals. Theoretically, BiOBr with a smaller Br:O ratio may possibly reduce its VB edge and then show a decrease in the band gap energy (Eg) and present stronger absorption in the visible light range than BiOBr. For instance, the synthesized $Bi_{24}O_{31}Br_{10}$ nanoflakes exhibit a stronger visible light absorption (band gap energy of 2.51 eV), larger BET surface area (40.1 m^2g^{-1}), and negatively charged surface, which results in a higher photocatalytic activity than that of three-dimensional (3D) BiOBr microspheres for TC degradation under visible light irradiation and is meaningful for future industrial applications.

3.4. Performance of bismuth-based metal oxides

Bismuth metal oxides (such as Bi_2WO_6, Bi_2MO_6, $BiVO_4$, and

Table 4
Comparison of the catalytic activity of bismuth-sulfides for antibiotic degradation.

Photocatalyst	Dosage	Light source	Antibiotics	Concentration/ volume of antibiotics	Preparation methods	Irradiation time/ degradation efficiency	References
Bi modified **Bi_2S_3** pillared g-C_3N_4photocatalyst	0.05 g	300 W Xe	tetracycline	10 mg L^{-1}/50 mL	solvothermal method	150 min/92.5%	Chen et al., 2017
flower-like BiOBr/**Bi_2S_3** composites	0.1 g	36 Watts, indoor fluorescent light	ciprofloxacin; ofloxacin	20 mg L^{-1}/100 mL	–	60 min/97.22%; 60 min/89.28%	Imam et al. (2020)
double Z-scheme $CuWO_4$/**Bi_2S_3**/ ZIF67 ternary heterostructure	0.3 g/L	LED (400 W/m^2, $\lambda > 400$ nm)	metronidazole (MTZ); cephalexin (CFX)	20 mg L^{-1}	hydro-thermal method	80 min/95.6% (MTZ); 90.1%(CFX)	Askari et al. (2020)
$LaTiO_2N$/**Bi_2S_3**Z-scheme nano heterostructures modified by rGO with high interfacial	0.03 g	300 W Xe	tetracycline	10 mg L^{-1}/100 mL	solvothermal method	90 min/96.4%	Sharma et al. (2020)

Table 5
Comparison of the catalytic activity of Bismuth oxyhalides for antibiotic degradation.

Photocatalyst	Dosage	Light source	Antibiotics	Concentration/ volume of antibiotics	Preparation methods	Irradiation time/ degradation efficiency	References
BiOI microspheres	0.05 g	1000 W Xe	tetracycline	15 mg L^{-1}/50 mL	a facile solution method at room temperature using PVP as surfactant	120 min/94%	Rong et al. (2012)
g-C_3N_4/**BiOBr** heterojunctions on carbon fibers	0.15 g	300 W Xe	tetracycline hydrochloride	20 mg L^{-1}/50 mL	a modified chemical bath deposition method	120 min/86.1%	Shi et al. (2020)
$Bi_4Ti_3O_{12}$/BiOBr heterojunction photocatalyst	–	300 W metal halide	ciprofloxacin	20 mg L^{-1}/100 mL	traditional solid state method combined with a successive in-situ growth method	120 min/96%	Shen et al. (2019)
biochar@$ZnFe_2O_4$/**BiOBr** Z-scheme heterojunction	0.05 g	300 W Xe	ciprofloxacin	15 mg L^{-1}/100 mL	solvothermal method	60 min/84%	Chen et al., 2019
tube-like S-scheme **BiOBr**/ BiO (HCOO)Br-x heterojunction	0.001 g	500 W Xe	tetracycline	20 mg L^{-1}/50 mL	coprecipitation method	120 min/80%	Imam et al. (2020)
graphene-like BN modified **BiOBr** flower-like materials	0.05 g	300 W Xe lamp	tetracycline; ciprofloxacin	20 mg L^{-1}/100 mL; 10 mg L^{-1}/100 mL	anionic liquid assisted solvothermal process.	80 min/70%; 80 min/81.5%	(Ji et al. (2016))
flake-shape **BiOBr**	0.02 g	400 W halogen	ciprofloxacin	5 mg L^{-1}/40 mL	hydrothermal method	140 min/100%	Zhang et al. (2015)
copper-doped **BiOBr** microflowers	0.01 g	200 W Xe	norfloxacin	10 mg L^{-1}/150 mL	solvothermal method	90 min/>99%	Lv et al. (2020)
a mesoporous spindle like $BiVO_4$/nanosheet **BiOCl** composite	0.05 g	150 W Xe	norfloxacin	5 mg L^{-1}/100 mL	hydrothermal method	60 min/ > 80%	Ma et al. (2017)
polyaniline/bismuth-rich bismuth oxyhalide composite	0.02 g	visible light (λ > 420 nm)	ciprofloxacin; tetracycline	10 mg L^{-1}/50 mL; 20 mg L^{-1}/50 mL	a facile solution method at room temperature	30 min/96.0% 50 min/99.0%; 10 min/73.0% 20 min/ 75.3% 240 min/85.7%	Xu et al. (2019)
BiOCl/g-C_3N_4/Cu_2O/Fe_3O_4	0.02 g	800 W Xe	sulfamethoxazole	100 μM/100 mL	facile co-precipitation method	60 min/99.5%	Kumar et al. (2018)

$Bi_2Ti_2O_7$) have been recently received substantial attention, comparable to that of bismuth oxyhalides, due to their potential application in the photocatalytic removal of recalcitrant pollutants, and detailed information on their behaviours and performances in antibiotic photocatalytic degradation is summarized in Table 6. These hybrid oxides exhibited a layered Aurivillius structure and were mainly composed of Bi_2O_3 and metal oxides, including V_2O_5, W_2O_3, Mo_2O_3, TiO_2, etc. (He et al., 2014). $BiVO_4$, a new η-type semiconductor, has been recommended for its high visible light-driven performance in the degradation of ciprofloxacin. Recent experimental results revealed that the efficiency of $BiVO_4$ was approximately four times higher than that of TiO_2 in ciprofloxacin degradation (Shi et al., 2013); specifically, its photocatalytic activity was highly dependent on its crystal phase. Similarly, nanocrystal and monoclinic-tetragonal $BiVO_4$ also exhibited excellent photoactivity in antibiotic removal, and as much as 67.61% of ciprofloxacin and 80.5% of tetracycline could be efficiently degraded in 60 min. Unfortunately, the light conversion efficiency of bismuth-based metal oxides is quite low, closely related to the fast recombination between electrons and holes.

Recently, a series of composite photocatalysts, such as g-C_3N_4/$BiVO_4$/RGO, $BiVO_4$/Z-scheme, Z-Scheme AgI/$Bi_4V_2O_{11}$ and $BiVO_4$/TiO_2/RGO heterojunction, have been successfully applied for antibiotic degradation (Table 6). Bi_2WO_6, with a band gap of 2.77 eV, is another typical η-type semiconductor belonging to the Aurivillius family with a structure composed of perovskite layers and has been prospectively used in heterogeneous photocatalysis for antibiotic degradation. The recent work of Zhu et al., 2020 found that the doping of Mg, Fe, Zn and Cu dramatically improved the photocatalytic degradation behaviour of Bi_2WO_6 for NOR (norfloxacin) and CIP removal, and as much as 89.44% of NOR and 99.11% of CIP could be removed by 1% Mg/Bi_2WO_6, closely related to its high specific surface area, strong electrostatic absorption, and significant photogeneration of $\bullet O_2^-$ and h^+. In contrast, others also pointed out that the doping of transition metals appears to expand the optical absorption, sometimes leading to an undesired instability and low quantum yield of photocatalytic reactions.

The photocatalytic degradation performance of other bismuth-based metal oxides for antibiotic removal was analysed and summarized in Table 6; these oxides exhibited an outstanding elimination efficiency and a slow reaction rate (>120 min). Generally, multiple bismuth compounds have frequently been applied to degrade organic pollutants under visible light radiation. Hailili et al. (2017) found that 3D flower-like $Bi_5FeTi_3O_{15}$ could achieve complete mineralization of antibiotics and reduced total organic carbon analysis with approximately 99.34% tetracycline removal in 60 min.

4. Effect of other pollutants on bismuth-based photocatalysts for antibiotic degradation

In addition to antibiotics, large quantities of anions (HCO_3^-, SO_4^{2-} and NO_3^-) and other organic pollutants (such as humic acid and fulvic acid) are also abundant within municipal wastewater (Parvez et al., 2013). Thus, the negative effect of those constituents on the bulk removal of antibiotics during photocatalytic degradation has been of great concern. The recent work of Zhao et al. (2019) found that the photocatalytic degradation efficiency of TC was seriously inhibited with increasing humic acid concentration within the g-C_3N_4 surface-decorated $Bi_2O_2CO_3$ photocatalytic degradation system, closely related to the reaction with active species (e.g., singlet oxygen) and the competitive absorption of short-wavelength photons under UV–vis irradiation. For comparison, Kumar et al. (2021) stated that the anions HCO_3^-, SO_4^{2-} and NO_3^- exhibited a detrimental effect on OFL (ofloxacin) degradation during the photocatalysis of the Z-scheme g-C_3N_4/$Bi_4Ti_3O_{12}$/$Bi_4O_5I_2$ heterojunction, and the inhibition rate decreased in the order SO_4^{2-} > HCO_3^- > NO_3^-. The corresponding interfering mechanisms of typical pollutants in wastewater on bulk photocatalysis are summarized and listed in Fig. 4. Briefly, HCO_3^- ions could inhibit degradation via the scavenging of •OH radicals. Similarly, anions such as Cl^-, SO_4^{2-} and NO_3^- could occupy the surface-active sites of bismuth-based compounds,

Table 6
Comparison of the catalytic activity of bismuth-based metal oxides for antibiotic degradation.

Photocatalyst	Dosage	Light Source	Antibiotics	Concentration/ Volume of Antibiotics	Preparation Methods	Irradiation Time/ Degradation Efficiency	References
$BiVO_4$ nanocrystal	0.15 g	150 W halogen	ciprofloxacin	10 mg L^{-1}/100 mL	a facile microwave-assisted method	60 min/67.61%	Shi et al. (2013)
monoclinic-tetragonal **$BiVO_4$**	0.1 g	150 W Xe	tetracycline	10 mg L^{-1}/100 mL	a facile microwave-assisted method	60 min/80.5%	Ming et al. (2015)
g-C_3N_4/**$BiVO_4$**/RGO	0.04 g	500 W halogen	ciprofloxacin	35 mg L^{-1}/40 mL	hydrothermal method	150 min/72%	Jiang et al. (2017)
$BiVO_4$/Z-scheme	–	300 W Xe	ciprofloxacin	10 mg L^{-1}/600 mL	a modified hydrothermal method	120 min/91.4%	Chen et al. (2018)
Z-Scheme AgI/**$Bi_4V_2O_{11}$**	0.1 g L^{-1}	–	sulfamethazine	10 mg L^{-1}	hydrothermal method and in-situ precipitation method	60 min/91.47%	Wen et al. (2020)
$BiVO_4$/TiO_2/RGO	–	1000 W Xe	chlortetracycline	10 mg L^{-1}	one-pot hydrothermal process	60 min/80.0%	(Zhu et al., 2017) Wei et al. (2019)
Bi_2WO_6/Ag_2O/CQDs	0.05 g	500 W Xe	tetracycline	20 mg L^{-1}/40 mL	precipitation process	60 min/>98%	Shen et al. (2018)
Bi_2WO_6 nanocuboids	0.075 g	150 W Philips CFL bulb, 1475 lux, 400–520 nm	levofloxacin	10 mg L^{-1}/100 mL	ultrasonic assisted hydrothermal method	150 min/80%	Kaur and Kansal (2016b)
CQDs/**Bi_2WO_6**	0.05 g	300 W Xe	ciprofloxacin	10 mg L^{-1}/100 mL	hydrothermal method	120 min/87%	Di et al. (2015)
BiOCl/Bi_2WO_6	0.1 g	300 W Xe	ciprofloxacin	10 mg L^{-1}/100 mL	a controlled anion exchange method	300 min/65%	Chen et al. (2016)
Bi_2WO_6/g-C_3N_4	0.1 g	300 W Xe	ceftriaxone sodium	10 mg L^{-1}/100 mL	hydrothermal method	120 min/94.5%	Zhang et al. (2018b)
metal-doped **Bi_2WO_6**	0.2 g	300 W Xe	norfloxacin	10 mg L^{-1}/200 mL	hydrothermal method	150 min/82.76%	Zhu et al. (2020)
mesoporous **Bi_2WO_6**	0.01 g	350 W Xe	tetracycline	20 mg L^{-1}/20 mL	hydrothermal method	120 min/97%	(Chu et al., 2016)
$Bi_2Ti_2O_7$/TiO_2/RGO	0.01 g	500 W Xe	ciprofloxacin	10 mg L^{-1}/40 mL	solvothermal method	180 min/85%	(Li et al., 2020)
Ag_3PO_4/**Bi_2WO_6**/Multi-Walled Carbon Nanotubes	0.03 g	1000 W Xe	norfloxacin	10 mg L^{-1}/50 mL	hydrothermal method and in-situ precipitation	180 min/94.34%	Zhu et al. (2020)
Z-scheme **BiO-xBr/$Bi_2O_2CO_3$**	0.01 g	500 W Xe	ciprofloxacin	40 mg L-1/40 mL	hydrothermal method	180 min/>90%	Ding et al. (2017b)
CdS–**Bi_2MoO_6**/RGO	0.02 g	500 W Xe	ciprofloxacin	20 mg L-1/40 mL	solvothermal method	60 min/91%	Chen et al. (2020)
$CaBiO_3$	0.03 g	100 W ABET Sunlite solar simulator	ciprofloxacin; tetracycline	10 mg L^{-1}/100 mL; 30 mg L^{-1}/100 mL	novel glycine-complexation method and conventional ion-exchange method	90 min/90.5%; 90 min/68.6%	Rokesh et al. (2020)
Ultrathin oxygen-vacancy abundant WO3decorated monolayer **Bi_2WO_6** nanosheet	0.04 g	300 W Xe	ciprofloxacin	10 mg L^{-1}/100 mL	hydrothermal method	120 min/79.6%	Zhang et al. (2019)
Anchoring single unit cell defect rich bismuth molybdate layers on ultrathin carbon nitride nanosheet	0.05 g	–	ciprofloxacin	50 mg L^{-1}/100 mL	CTAB-assisted hydrothermal method	120 min/77.95%	Li et al. (2020a)
3D flower-like **$Bi_5FeTi_3O_{15}$**	0.04 g	300 W Xe	tetracycline	$1*10^{-5}$ mol L^{-1}/ 100 mL	hydrothermal synthesis	60 min/99.34%	Hailili et al. (2017)

further restricting •OH generation and affecting the interactions of antibiotics with the catalysts (Yang et al., 2018). Interestingly, a low concentration of NO_3^- may somehow enhance the degradation of antibiotics; for instance, the recent work of Guo et al. (2017) reported that the rate constant increases from 0.0583 min^{-1} to 0.0751 min^{-1} when the nitrate concentration increases from 0.3 mM to 3 mM during the catalysis of BiOBr/iron oxides. However, a significant inhibition was observed once the concentration of NO_3^- reached 7 mM. Thus, it is urgent to develop new coupled approaches with bismuth-based catalysts to promote the generation of reactive oxygen species, which is beneficial for antibiotic photocatalytic degradation and to reduce the prevalence of conventional contaminants.

5. Photocatalytic degradation enhancement of bismuth-based catalysts for antibiotic and ARB removal

5.1. Coupling process for efficiency enhancement of bismuth-based photocatalysts

Recently, a series of novel processes coupled with bismuth-based catalysts have been developed for antibiotic degradation (Fig. 5). For example, recent work demonstrated that the introduction of H_2O_2 into the SSL/Bi_2WO_6 photocatalytic system (SSL/Bi_2WO_6/H_2O_2) can significantly enhance the degradation efficiency of norfloxacin. As much as 79.4% of norfloxacin was degraded within 12 min (11.4% higher than the system with only SSL/Bi_2WO_6), which was ascribed to the synergetic role of H_2O_2 (Song et al., 2006). Simultaneously, the e^- generated from the Bi_2WO_6 photocatalytic reaction could be efficiently captured by

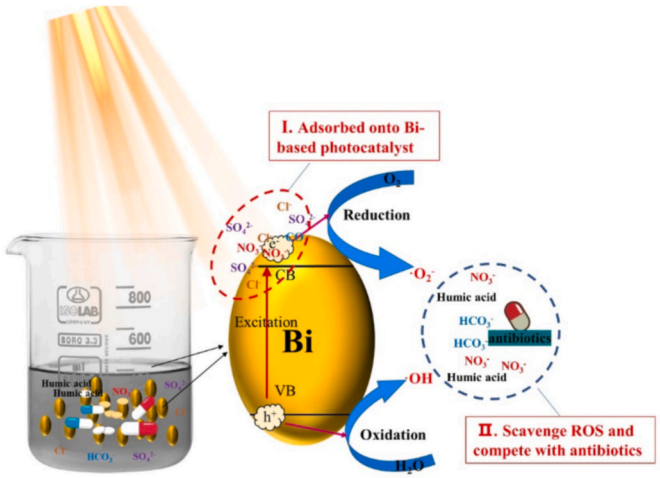

Fig. 4. Interfering mechanisms of typical constituents in actual wastewater on bismuth-based catalyst photocatalytic degradation.

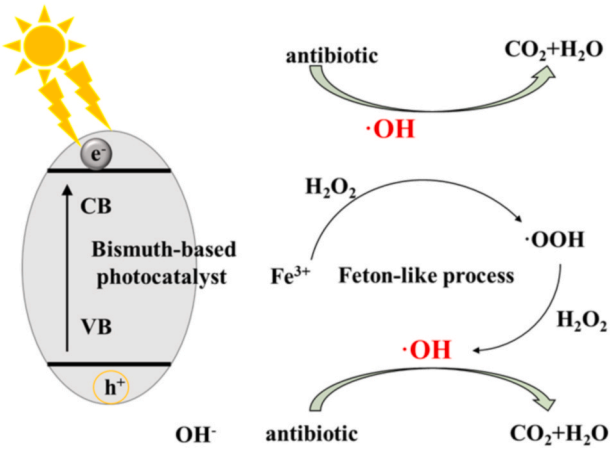

Fig. 5. The mechanism of coupled processes with bismuth-based compounds for antibiotic degradation.

H_2O_2 and gave rise to •OH radicals while benefiting the separation of photo-generated e^- and h^+ from the Bi_2WO_6 surface. Undoubtedly, increasing the number available h^+ with its longer lifetime would improve norfloxacin decay via new •OH radical generation (Chen and Chu, 2016). Furthermore, some researchers have attempted to modify bismuth-based photocatalysts to construct a heterogeneous photo-Fenton system to improve the degradation efficiency of antibiotics. For instance, Chen et al. (2013) found that the SSL/(C/Fe–Bi_2WO_6)/H_2O_2 system exhibited excellent norfloxacin decay, in which 97% of norfloxacin was degraded after 1 h photocatalytic degradation. Yi et al. (2018) combined an environmentally friendly biomimetic material hemin and Bi_2WO_6 to obtain a novel hemin-modified Bi_2WO_6 (H–Bi_2WO_6) photocatalyst and found that the photocatalytic Fenton-like process showed a 99.5% degradation efficiency of rhodamine B (RhB) under simulated solar light irradiation (SSL/H–Bi_2WO_6/H_2O_2). However, its efficiency for antibiotic degradation should be further explored.

5.2. ARB removal during bismuth-based catalyst photocatalytic degradation

Recently, there has been growing pressure for wastewater treatment plants to mitigate the discharge of antibiotic-resistant bacteria (ARB) and extracellular resistance genes (eARGs), in addition to antibiotics. As mentioned above, bismuth-based catalysts can generate reactive oxygen species (ROS), such as h^+, •OH, and $•O_2^-$ in the visible right region, and these ROS can destroy the cell membrane of bacteria and enter the cell to oxidize/damage proteins and nucleic acids (Fig. 6). Xiang et al. (2016) revealed that 30%BiOI/$BiVO_4$ composite photocatalysts exhibited excellent photocatalytic antibacterial activities for *P. aeruginosa* (with an antibacterial rate of 99.99%), wherein $•O_2^-$ and h^+ were the main reactive species. Zhang et al. (2010) synthesized visible light-driven (VLD) AgBr–Ag–Bi_2WO_6 nanojunctions and found that 5×10^7 CFU (colony-forming units) mL^{-1} *E. coli* K-12 could be completely inactivated within 15 min. However, antibiotic-resistant bacteria (ARB) usually display a stronger resistance to disinfection methods than bacterial populations (Mao et al., 2015); thus, the performance of bismuth-based catalysts on ARB and ARGs should be of great concern. Recently, Li et al., 2020a, 2020b, 2020c, 2020d constructed hierarchical $Bi_2O_2CO_3$ microspheres wrapped with nitrogen-doped reduced graphene oxide (NRGO) to enhance the inactivation/degradation of multidrug-resistant *E. coli* NDM-1 (New Delhi metallo-β-lactamase 1) and plasmid-encoded ARG (blaNDM-1) in secondary effluent and proven their feasibility in ARG removal. Specifically, NGWM (NRGO-wrapped $Bi_2O_2CO_3$ microspheres) showed a much higher decay efficiency of ARB in secondary effluent ($3.08 \pm 0.27 \times 10^8$ CFU/mg catalyst) than Bi2O2CO3 microspheres ($0.78 \pm 0.09 \times 10^8$ CFU/mg catalyst) and GWM ($2.07 \pm 0.18 \times 10^8$ CFU/mg catalyst). Moreover, other novel visible light-driven photocatalysts (as shown in Table 7) were also explored for the improvement of antibiotic degradation. In comparison with other visible light-driven catalysts, bismuth-based photo-catalysts exhibited the advantages of low production cost, high photostability, narrow band gap, resistance to photo-corrosion, large specific area/pore volume and so on. Thus, more attention should be given to declaring the removal mechanism of ARB by bismuth-based compounds and further enhancing ARG elimination.

6. Conclusion and perspectives

Great advantages have been observed when using bismuth-based photocatalysts for antibiotic photocatalytic degradation. In this review, the performance, mechanisms and pathways of bismuth-based compounds related photocatalytic degradation for typical antibiotic removal are summarized. In general, single-component bismuth-based photocatalysts exhibit a narrow light absorption range and weak redox ability. Thus, modified bismuth-based compounds have been extensively investigated via morphology/structure mediation, heterojunction construction, and element doping and have shown better performance in antibiotic photocatalytic degradation. Although remarkable results have been achieved in the field in bismuth-based photocatalysts for antibiotic removal, tough challenges, such as the existence of multiple sources of

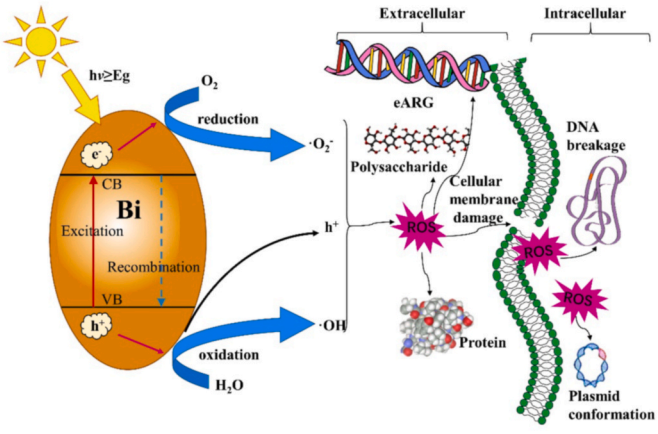

Fig. 6. The mechanism of sterilization by bismuth-based photocatalysts.

Table 7
Comparison of the catalytic activity of other visible-light-driven photocatalysts for ARB and ARGs elimination.

Photocatalyst	Dosage	Light source	ARG/ARB	Initial copies of ARGs or bacterial concentration	Degradation efficiency and irradiation time/	References
g-C_3N_4	5 g/L	a Xenon lamp equipped with a 400 nm optical filter	ARB: CIP-resistant ARB (*Raoultella planticola* (NR112011.1), *Escherichia coli* (KU156692.1), *Escherichia coli* (NR136472.1)), OFL-resistant ARB (*Escherichia coli* (KP, 181716.1))	1.5×10^8 CFU/mL	At 60 min, the inactivation of the ARB isolates was in the range of 0.31–0.41log.	Ding et al. (2019)
Ag/AgBr/g-C_3N_4	211 mg/L	a 500 W Xenon arc lamp with a cutoff filter ($\lambda <$ 420 nm)	ARB: tetracycline (TC)-resistant *Escherichia coli* (TC-E. coli) ARG:TC-resistant genes (TC-RGs): three TC-RGs (*ter*A, *ter*M, and *tet*Q) and the class 1 integron gene *int*l1	10^7 CFU/mL	ARB:6.1 log after 90 min ARGs: 49%, 86%, 69%, and 86% for *tet*A, *ter*M, *tet*Q,and *intl*1, respectively.	Yu et al. (2020)
TiO_2/Ag/GO nanocomposites	100 mg/L	500 W Xenon lamp	ARB: *E. coli HB10663* (resistance to tetracycline and gentamicin), *E. coli HB10667* (resistance to streptomycin) and *E. coli HB101* (resistance to kanamycin, tetracycline, and ampicillin)	10^8 CFU/mL	87.8% in 10 min under simulated sunlight irradiation.	(Guo M T and Tian X B. 2019)
Ag/TiO_2/graphene oxide (GO) combined with a polyvinylidene fluoride (PVDF) ultrafiltration membrane	–	300 W Xe lamp	ARGs: *tet*A and *amp*C	–	99.99% within 30 min	Zhou et al., 2020

pollutants within wastewater, the complex characteristics of antibiotics, the potential threat of ARGs, and difficulties in implementing bismuth-based photocatalysts for intermediate and ARG removal, are also faced during the practical application of bismuth-based photocatalysts. Thus, we recommend the following research directions:

First, the evaluation of photocatalytic degradation by bismuth-based catalysts has mostly been conducted in synthetic solutions with antibiotic concentrations under the level of mg/L. Actually, the concentration of antibiotics in surface water and wastewater treatment plant effluents is usually at the level of μg/L or ng/L. Thus, applying bismuth-based photocatalysts for practical applications of antibiotic degradation, especially for conditions with trace antibiotics, should be of great concern.

Second, considering that hydroxyl radicals exhibited a stronger oxidation potential but were less selective, the reaction pathway between hydroxyl radicals and contaminants was mainly ascribed to adsorption on the surface of catalysts. Future studies should pay attention to the absorbability of bismuth-based catalysts for antibiotic removal and the interference of other pollutants.

Third, the degradation pathway provides a clear illumination of the fate and transformation of antibiotics during the photocatalytic degradation process. Thus, exploring the photocatalytic degradation mechanism in depth at the atomic level is compulsory for promoting the efficiency of antibiotic degradation.

Fourth, anions in real water matrices exerted a negative influence on antibiotic removal during bismuth-based catalyst photodegradation. For this reason, catalysts that have excellent anti-influence ability on inorganic salts should be developed.

Fifth, in addition to concern about antibiotics, there is growing pressure for wastewater treatment plants to mitigate the discharge of ARB and eARGs. It is urgent to develop a new technical route for the simultaneous removal of antibiotics and ARB or ARGs by bismuth-based photocatalysts. Thus, coupling photocatalysis with other treatments, such as electrocatalysis, the Fenton process, and biodegradation, should be further explored.

Finally, the loss of heavy metal elements (such as ZnO and Ag) from bismuth-based heterojunctions, via photo-corrosion, from photocatalysts into the solution either prior to or after irradiation may be of greater harm to humans than antibiotics; thus, their toxicity should be of great concern.

Author contribution

Kena Qin: Writing – original draft. Qingliang Zhao: Writing – original draft. Hang Yu: Writing – original draft. Xinhui Xia: Visualization, Writing – original draft. Jianju Li: Visualization, Writing – original draft. Shufei He: Visualization, Writing – original draft. Liangliang Wei: Writing – review & editing. Taicheng An: Writing – review & editing.

Declaration of competing interest

The authors declare that they have no known competing financial interests or personal relationships that could have appeared to influence the work reported in this paper.

Acknowledgements

This work was supported by the funding from the National Nature Science Foundation of China (No. 51878213). The National Key Research and Development Program of China (2018YFC0406303). The State Key Laboratory of Urban Water Resource and Environment (No. 2020TS01). The Heilongjiang Nature Science Foundation (YQ 2020E022). HIT Environment and Ecology Innovation Special Funds (No. HSCJ201611). Sub-project of the National Key Research and Development Program (2016YFC0401106-01).

References

Ajiboye, T.O., et al., 2021. The performance of bismuth-based compounds in photocatalytic applications. Surfaces and Interfaces 23, 100927. https://doi.org/10.1016/j.surfin.2021.100927.

An, J., et al., 2015. Photocatalytic degradation of three amantadine antiviral drugs as well as their eco-toxicity evolution. Catal. Today 258, 602–609. https://doi.org/10.1016/j.cattod.2015.01.004.

An, T., et al., 2010a. Kinetics and mechanism of advanced oxidation processes (AOPs) in degradation of ciprofloxacin in water. Appl. Catal. B Environ. 94, 288–294. https://doi.org/10.1016/j.apcatb.2009.12.002.

An, T., et al., 2010b. Mechanistic considerations for the advanced oxidation treatment of fluoroquinolone pharmaceutical compounds using TiO_2 heterogeneous catalysis. J. Phys. Chem. 114, 2569–2575. https://doi.org/10.1021/jp911349y.

Antoñanzas, F., Goossens, H., 2019. The economics of antibiotic resistance: a claim for personalised treatments. Eur. J. Health Econ. 20, 483–485. https://doi.org/10.1007/s10198-018-1021-z.

Askari, N., et al., 2020. Fabrication of $CuWO_4$/Bi_2S_3/ZIF67 MOF: a novel double Z-scheme ternary heterostructure for boosting visible-light photodegradation of antibiotics. Chemosphere 251, 126453. https://doi.org/10.1016/j.chemosphere.2020.126453.

Bao, et al., 2018. Novel Z-scheme BiOBr/reduced graphene oxide/protonated g-C_3N_4 photo-catalyst: synthesis, characterization, visible light photocatalytic activity and mechanism. Appl. Surf. Sci. 437, 51–61. https://doi.org/10.1016/j.apsusc.2017.12.075.

Berendonk, T.U., et al., 2015. Tackling antibiotic resistance: the environmental framework. Nat. Rev. Microbiol. 13, 310–317. https://doi.org/10.1038/nrmicro3439.

Bi, J., et al., 2007. Simple solvothermal routes to synthesize nanocrystalline Bi_2MoO_6 photocatalysts with different morphologies. Acta Mater. 55, 4699–4705. https://doi.org/10.1016/j.actamat.2007.04.034.

Boruah, B., et al., 2019. Novel insights into the properties of $AgBi_3$ photocatalyst and its application in immobilized state for 4-nitrophenol degradation and bacteria inactivation. J. Photochem. Photobiol. Chem. 373, 105–115. https://doi.org/10.1016/j.jphotochem.2018.11.001.

Chen, et al., 2016. Synthesis of chemically bonded BiOCl@Bi_2WO_6 microspheres with exposed (020) Bi_2WO_6 facets and their enhanced photocatalytic activities under visible light irradiation. Appl. Surf. Sci. 361, 63–71. https://doi.org/10.1016/j.apsusc.2015.11.130.

Chen, D., et al., 2017. Fabrication of Bi modified Bi_2S_3 pillared g-C_3N_4 photocatalyst and its efficient photocatalytic reduction and oxidation performances. Appl. Surf. Sci. 426, 427–436. https://doi.org/10.1016/j.apsusc.2017.07.139.

Chen, F., et al., 2017. Achieving UV and visible-light photocatalytic activity enhancement of AgI/$BiOIO_3$ heterostructure: decomposition for diverse industrial contaminants and high mineralization ability. Chin. Chem. Lett. 28 (12), 2244–2250. https://doi.org/10.1016/j.cclet.2017.09.017.

Chen, F., et al., 2018. Efficient construction of bismuth vanadate-based Z-scheme photocatalyst for simultaneous Cr (VI) reduction and ciprofloxacin oxidation under visible light: kinetics, degradation pathways and mechanism. Chem. Eng. J. 348, 157–170. https://doi.org/10.1016/j.cej.2018.04.170.

Chen, M., et al., 2019. Solvothermal synthesis of biochar@$ZnFe_2O_4$/BiOBr Z-scheme heterojunction for efficient photocatalytic ciprofloxacin degradation under visible light. Appl. Surf. Sci. 493, 1361–1367. https://doi.org/10.1016/j.apsusc.2019.04.160.

Chen, M., Chu, W., 2016. H_2O_2 assisted degradation of antibiotic norfloxacin over simulated solar light mediated Bi_2WO_6: kinetics and reaction pathway. Chem. Eng. J. 296, 310–318. https://doi.org/10.1016/j.cej.2016.03.083.

Chen, P., et al., 2019. Phosphate-modified m-Bi_2O_4 enhances the absorption and photocatalytic activities of sulfonamide: mechanism, reactive species, and reactive sites. J. Hazard Mater. 384, 121443. https://doi.org/10.1016/j.jhazmat.2019.121443.

Chen, S., et al., 2013. Preparation, characterization of C/Fe-Bi_2WO_6 nanosheet composite and degradation application of norfloxacin in water. J. Nanosci. Nanotechnol. 13, 5624–5630. https://doi.org/10.1166/jnn.2013.7486.

Chen, Z., et al., 2020. CdS-Bi_2MoO_6/RGO nanocomposites for efficient degradation of ciprofloxacin under visible light. J. Mater. Sci. 55, 6065–6077. https://doi.org/10.1007/s10853-020-04413-z.

Cheng, Z., Hu, X., 2017. Performance and degradation mechanism of a sequencing batch biofilm reactor combined with an electrochemical process for the removal of low concentrations of cefuroxime. Chem. Eng. J. 320, 93–103. https://doi.org/10.1016/j.cej.2017.03.037.

Chu, X., et al., 2016. Effective degradation of tetracycline by mesoporous Bi_2WO_6 under visible light irradiation. Front. Environ. Sci. Eng. 10, 211–218. https://doi.org/10.1007/s11783-014-0753-y.

Daghrir, R., Drogui, P., 2013. Tetracycline antibiotics in the environment: a review. Environ. Chem. Lett. 11, 209–227. https://doi.org/10.1007/s10311-013-0404-8.

Dai, G., et al., 2012. A new approach for photo-corrosion inhibition of Ag_2CO_3 photocatalyst with highly visible-light-responsive reactivity. J. Phys. Chem. C 116, 15519–15524. https://doi.org/10.1021/jp305669f.

Di, J., et al., 2015. Novel visible-light-driven CQDs/Bi_2WO_6 hybrid materials with enhanced photocatalytic activity toward organic pollutants degradation and mechanism insight. Appl. Catal. B Environ. 168, 51–61. https://doi.org/10.1016/j.apcatb.2014.11.057.

Ding, J., et al., 2017. Z-scheme BiO1-xBr/$Bi_2O_2CO_3$ photocatalyst with rich oxygen vacancy as electron mediator for highly efficient degradation of antibiotics. Appl. Catal. B Environ. 205, 281–291. https://doi.org/10.1016/j.apcatb.2016.12.018.

Ding, N., et al., 2019. Enhanced inactivation of antibiotic-resistant bacteria isolated from secondary effluents by g-C_3N_4 photocatalysis. Environ. Sci. Pollut. Control Ser. 26 (18), 18730–18738. https://doi.org/10.1007/s11356-019-05080-7.

Fang, W., Shangguan, W., 2019. A review on bismuth-based composite oxides for photocatalytic hydrogen generation. Int. J. Hydrogen Energy 44, 895–912. https://doi.org/10.1016/j.ijhydene.2018.11.063.

Giles, A., et al., 2019. Sulfonamide allergies. Pharmacy 7, 132. https://doi.org/10.3390/pharmacy7030132.

Guo, C., et al., 2017. Assessing the photocatalytic transformation of norfloxacin by BiOBr/iron oxides hybrid photocatalyst: kinetics, intermediates, and influencing factors. Appl. Catal. B Environ. 205, 68–77. https://doi.org/10.1016/j.apcatb.2016.12.032.

Guo, M., Tian, X., 2019. Impacts on antibiotic-resistant bacteria and their horizontal gene transfer by graphene-based TiO_2&Ag composite photocatalysts under solar irradiation. J. Hazard Mater. 380, 120877. https://doi.org/10.1016/j.jhazmat.2019.120877.

Gurunathan, K., 2004. Photocatalytic hydrogen production using transition metal ions-doped gamma-Bi_2O_3 semiconductor particles. Int. J. Hydrogen Energy 29, 933–940. https://doi.org/10.1016/j.ijhydene.2003.04.001.

Hailili, R., et al., 2017. Layered nanostructured ferroelectric perovskite $Bi_5FeTi_3O_{15}$ for visible light photodegradation of antibiotics. J. Mater. Chem. 5, 21275–21290. https://doi.org/10.1039/C7TA06618J.

Hao, R., et al., 2012. Efficient adsorption and visible-light photocatalytic degradation of tetracycline hydrochloride using mesoporous BiOI microspheres. J. Hazard Mater. 209–210, 137–145. https://doi.org/10.1016/j.jhazmat.2012.01.006.

He, R., et al., 2014. Recent advances in visible light Bi-based photocatalysts. Chin. J. Catal. 35, 989–1007. https://doi.org/10.1016/S1872-2067(14)60075-9.

Ho, C., et al., 2013. The study of optical band edge property of bismuth oxide nanowires α-Bi_2O_3. Opt Express 21, 11965–11972. https://doi.org/10.1364/OE.21.011965.

Homem, V., Santos, L., 2011. Degradation and removal methods of antibiotics from aqueous matrices - a review. J. Environ. Manag. 92, 2304–2347. https://doi.org/10.1016/j.jenvman.2011.05.023.

Huang, Z., et al., 2014. Nanostructured bismuth vanadate-based materials for so-lar-energy-driven water oxidation: a review on recent progress. Nanoscale 6, 14044–14063. https://doi.org/10.1039/C4NR05245E.

Huo, Y., et al., 2012. Solvothermal synthesis of flower-like BiOBr microspheres with highly visible-light photocatalytic performances. Appl. Catal. B Environ. 111, 334–341. https://doi.org/10.1016/j.apcatb.2011.10.016.

Imam, S.S., et al., 2020. Room-temperature synthesis of flower-like BiOBr/Bi_2S_3 composites for the catalytic degradation of fluoroquinolones using indoor fluorescent light illumination. Colloid. Surface. Physicochem. Eng. Aspect. 585, 124069. https://doi.org/10.1016/j.colsurfa.2019.124069.

Ji, et al., 2016. Advanced photocatalytic performance of graphene-like BN modified BiOBr flower-like materials for the removal of pollutants and mechanism insight. Appl. Catal. B Environ. 183, 254–262. https://doi.org/10.1016/j.apcatb.2015.10.036.

Jiang, D., et al., 2017. RGO-promoted all-solid-state g-C_3N_4/$BiVO_4$ Z-scheme heterostructure with enhanced photocatalytic activity toward the degradation of antibiotics. Ind. Eng. Chem. Res. 56, 8823–8832. https://doi.org/10.1021/acs.iecr.7b01840.

Kaur, A., Kansal, S.K., 2016. Bi_2WO_6 nanocuboids: an efficient visible light active photocatalyst for the degradation of levofloxacin drug in aqueous phase. Chem. Eng. J. 302, 194–203. https://doi.org/10.1016/j.cej.2016.05.010.

Kumar, A., et al., 2018. Quaternary magnetic BiOCl/g-C_3N_4/Cu_2O/Fe_3O_4 nano-junction for visible light and solar powered degradation of sulfamethoxazole from aqueous environment. Chem. Eng. J. 334, 462–478. https://doi.org/10.1016/j.cej.2017.10.049.

Kumar, A., et al., 2021. Construction of dual Z-scheme g-C_3N_4/$Bi_4Ti_3O_{12}$/$Bi_4O_5I_2$ heterojunction for visible and solar powered coupled photocatalytic antibiotic degradation and hydrogen production: boosting via I^-/I^{3-} and Bi^{3+}/Bi^{5+} redox mediators. Appl. Catal. B Environ. 284 https://doi.org/10.1016/j.apcatb.2020.119808, 119808.

Li, B., et al., 2018. $BiVO_4$ quantum dot-decorated $BiPO_4$ nanorods 0D/1D heterojunction for enhanced visible-light-driven photocatalysis. Dalton Trans. 47 (30), 10288–10298. https://doi.org/10.1039/C8DT02402B.

Lee, Y., von Gunten, U., 2012. Quantitative structure-activity relationships (QSARs) for the transformation of organic micropollutants during oxidative water treatment. Water Res. 46, 6177–6195. https://doi.org/10.1016/j.watres.2012.06.006.

Li, B., et al., 2020a. Anchoring single-unit-cell defect-rich bismuth molybdate layers on ultrathin carbon nitride nanosheet with boosted charge transfer for efficient photocatalytic ciprofloxacin degradation. J. Colloid Interface Sci. 560, 701–713. https://doi.org/10.1016/j.jcis.2019.10.116.

Li, W., et al., 2020b. $Bi_2Ti_2O_7$/TiO_2/RGO composite for the simulated sunlight-driven photocatalytic degradation of ciprofloxacin. Mater. Chem. Phys. 256, 123650. https://doi.org/10.1016/j.matchemphys.2020.123650.

Li, Z., et al., 2020c. Bismuth chromate (Bi_2CrO_6): a promising semiconductor in photocatalysis. J. Catal. 382, 40–48. https://doi.org/10.1016/j.jcat.2019.12.001.

Ling, C., et al., 2020. Enhanced removal of sulfamethoxazole by a novel composite of TiO_2 nanocrystals in situ wrapped-Bi_2O_4 microrods under simulated solar irradiation. Chem. Eng. J. 384, 123278. https://doi.org/10.1016/j.cej.2019.123278.

Li, D., et al., 2020d. Hierarchical $Bi_2O_2CO_3$ wrapped with modified graphene oxide for adsorption-enhanced photocatalytic inactivation of antibiotic resistant bacteria and resistance genes. Water Res. 184, 116157. https://doi.org/10.1016/j.watres.2020.116157.

Li, X., et al., 2018. Constructing photocatalyst from β-Bi_2O_3 photonic crystals for enhanced photocatalytic performance. J. Porous Mater. 25, 677–685. https://doi.org/10.1007/s10934-017-0480-4.

Liu, J., et al., 2013. Correlation of crystal structures and electronic structures with visible light photocatalytic properties of $NaBiO_3$. Chem. Phys. Lett. 572, 101–105. https://doi.org/10.1016/j.cplett.2013.04.040.

Liu, Y., et al., 2017. A novel synergy of Er^{3+}/Fe^{3+} co-doped porous Bi_5O_7I microspheres with enhanced photocatalytic activity under visible-light irradiation. Appl. Catal. B Environ. 205, 421–432. https://doi.org/10.1016/j.apcatb.2016.12.061.

Liu, Z., et al., 2017. Aqueous tetracycline degradation by coal-based carbon electrocatalytic filtration membrane: effect of nano antimony-doped tin dioxide coating. Chem. Eng. J. 314, 59–68. https://doi.org/10.1016/j.cej.2016.12.093.

Lou, S.N., et al., 2018. Concentration-mediated band gap reduction of Bi_2MoO_6 photoanodes prepared by Bi^{3+} cation insertions into anodized MoO_3 thin films: structural, optical and photoelectrochemical properties. ACS Appl. Energy Mater. 1, 3955–3964. https://doi.org/10.1021/acsaem.8b00675.

Lv, X., et al., 2020. Solvothermal synthesis of copper-doped BiOBr microflowers with enhanced adsorption and visible-light driven photocatalytic degradation of norfloxacin. Chem. Eng. J. 401, 126012. https://doi.org/10.1016/j.cej.2020.126012.

Ma, X., et al., 2017. Preparation of $BiVO_4$/BiOCl heterojunction photocatalyst by in-situ transformation method for norfloxacin photocatalytic degradation. J. Alloys Compd. 702, 68–74. https://doi.org/10.1016/j.jallcom.2017.01.214.

Ma, X., et al., 2020. Preparation of $BiOCl_{0.9}I_{0.1}$/β-Bi_2O_3 composite for degradation of tetracycline hydrochloride under simulated sunlight. Chin. J. Catal. 41, 1535–1543. https://doi.org/10.1016/S1872-2067(19)63486-8.

Malathi, A., et al., 2018. A review on $BiVO_4$ photocatalyst: activity enhancement methods for solar photocatalytic applications. Appl. Catal. Gen. 555, 47–74. https://doi.org/10.1016/j.apcata.2018.02.010.

Mao, D., et al., 2015. Prevalence and proliferation of antibiotic resistance genes in two municipal wastewater treatment plants. Water Res. 85, 458–466. https://doi.org/10.1016/j.watres.2015.09.010.

Meredith, H.R., et al., 2015. Collective antibiotic tolerance: mechanisms, dynamics and intervention. Nat. Chem. Biol. 11, 182. https://doi.org/10.1038/nchembio.1754.

Ming, Y., et al., 2015. Microwave-assisted synthesis of monoclinic-tetragonal $BiVO_4$ heterojunctions with enhanced visible-light-driven photocatalytic degradation of tetracycline. RSC Adv. 5, 90255–90264. https://doi.org/10.1039/C5RA13684A.

Mohammad-AliShahbazi, et al., 2020. The versatile biomedical applications of bismuth-based nanoparticles and composites: therapeutic, diagnostic, biosensing, and regenerative properties. Chem. Soc. Rev. 49, 1253–1321. https://doi.org/10.1039/C9CS00283A.

Murugesan, S., et al., 2010. Band-engineered bismuth titanate pyrochlores for visible light photocatalysis. J. Phys. Chem. C 114, 10598–10605. https://doi.org/10.1021/jp906252r.

Nabi, I., et al., 2019. A comparative study of bismuth-based photocatalysts with titanium dioxide for perfluorooctanoic acid degradation. Chin. Chem. Lett. 30 (12), 2225–2230. https://doi.org/10.1016/j.cclet.2019.07.058.

Nogueira, A.E., et al., 2014. Synthesis and photocatalytic properties of bismuth titanate with different structures via oxidant peroxo method (OPM). J. Colloid Interface Sci. 415, 89–94. https://doi.org/10.1016/j.jcis.2013.10.010.

Niu, J., et al., 2013. Effects of environmental factors on sulfamethoxazole photodegradation under simulated sunlight irradiation: kinetics and mechanism. J. Environ. Sci. 25 (6), 1098–1106. https://doi.org/10.1016/S1001-0742(12)60167-3.

Parvez, M., et al., 2013. Evaluating the wastewater impacts on groundwater and irrigated soil. World Appl. Sci. J. 24, 1184–1191. https://doi.org/10.5829/idosi.wasj.2013.24.09.922.

Patel, M., et al., 2019. Pharmaceuticals of emerging concern in aquatic systems: chemistry, occurrence, effects, and removal methods. Chem. Rev. 119, 3510–3673. https://doi.org/10.1021/acs.chemrev.8b00299.

Ponraj, C., et al., 2017. A review on the visible light active $BiFeO_3$ nanostructures as suitable photocatalyst in the degradation of different textile dyes. Environmental Nanotechnology, Monitoring & Management 7, 110–120. https://doi.org/10.1016/j.enmm.2017.02.001.

Qin, K., et al., 2020a. A review of ARGs in WWTPs: sources, stressors and elimination. Chin. Chem. Lett. 31, 2603–2613. https://doi.org/10.1016/j.cclet.2020.04.057.

Qin, K., et al., 2020b. Removal trends of sulfonamides and their ARGs during soil aquifer treatment and subsequent chlorination: effect of aerobic and anaerobic biodegradation. Environ. Sci.: Water Research & Technology 6, 2331–2340. https://doi.org/10.1039/D0EW00270D.

Ramachandran, et al., 2011. Photocatalytic properties of $KBiO_3$ and $LiBiO_3$ with tunnel structures. J. Chem. Soc. B 123, 517–524. https://doi.org/10.1007/s12039-011-0080-9.

Ren, A., et al., 2014. Enhanced visible-light-driven photocatalytic activity for antibiotic degradation using magnetic $NiFe_2O_4/Bi_2O_3$ heterostructures. Chem. Eng. J. 258, 301–308. https://doi.org/10.1016/j.cej.2014.07.071.

Rokesh, K., et al., 2020. Calcium bismuthate ($CaBiO_3$): a potential sunlight-driven perovskite photocatalyst for the degradation of emerging pharmaceutical contaminants. Chemphotochem 4, 373–380. https://doi.org/10.1002/cptc.201900265.

Rong, H., et al., 2012. Efficient adsorption and visible-light photocatalytic degradation of tetracycline hydrochloride using mesoporous BiOI microspheres. J. Hazard Mater. 137–145. https://doi.org/10.1016/j.jhazmat.2012.01.006.

Sánchez-Martínez, D., et al., 2016. Photocatalytic properties of Bi_2O_3 powders obtained by an ultrasound-assisted precipitation method. Ceram. Int. 42, 2013–2020. https://doi.org/10.1016/j.ceramint.2015.10.007.

Schlesinger, M., et al., 2013. Metastable β-Bi_2O_3 nanoparticles with potential for photocatalytic water purification using visible light irradiation. Chemistryopen 2, 146–155. https://doi.org/10.1002/open.201300013.

Shahbazi, M., et al., 2020. The versatile biomedical applications of bismuth-based nanoparticles and composites: therapeutic, diagnostic, biosensing, and regenerative properties. Chem. Soc. Rev. 49, 1253–1321. https://doi.org/10.1039/C9CS00283A.

Sharma, S.K., et al., 2020. $LaTiO_2N/Bi_2S_3$ Z-scheme nano heterostructures modified by rGO with high interfacial contact for rapid photocatalytic degradation of tetracycline. J. Mol. Liq. 311, 113300. https://doi.org/10.1016/j.molliq.2020.113300.

Shen, G., et al., 2019. Enhanced visible light photocatalytic performance of a novel hetero-structured $Bi_4Ti_3O_{12}$/BiOBr photocatalyst. New J. Chem. 43, 12932–12940. https://doi.org/10.1039/C9NJ02723H.

Shen, J., et al., 2018. Construction of 3D marigold-like Bi_2WO_6/Ag_2O/CQDs heterostructure with superior visible-light active photocatalytic activity toward tetracycline degradation and selective oxidation. J. Mater. Sci. 53, 12040–12055. https://doi.org/10.1007/s10853-018-2479-x.

Shi, W., et al., 2013. Microwave-assisted synthesis of nano-scale $BiVO_4$ photocatalysts and their excellent visible-light-driven photocatalytic activity for the degradation of ciprofloxacin. Chem. Eng. J. 215, 740–746. https://doi.org/10.1016/j.cej.2012.10.071.

Shi, W., et al., 2020. Three-dimensional Z-Scheme $Ag_3PO_4/Co_3(PO_4)_2$@Ag heterojunction for improved visible-light photocatalytic degradation activity of tetracycline. J. Alloys Compd. 818, 152883. https://doi.org/10.1016/j.jallcom.2019.152883.

Shi, Z., et al., 2020. Fabrication of g-C_3N_4/BiOBr heterojunctions on carbon fibers as weaveable photocatalyst for degrading tetracycline hydrochloride under visible light. Chem. Eng. J. 386, 124010. https://doi.org/10.1016/j.cej.2020.124010.

Singh, S., et al., 2018. A review and recent developments on strategies to improve the photocatalytic elimination of organic dye pollutants by BiOX (X= Cl, Br, I, F) nanostructures. Kor. J. Chem. Eng. 35, 1955–1968. https://doi.org/10.1007/s11814-018-0112-y.

Sivakumar, A., et al., 2014. A review on decolourisation of dyes by photodegradation using various bismuth catalysts. Journal of the Taiwan Institute of Chemical Engineers 45, 2300–2306. https://doi.org/10.1016/j.jtice.2014.07.003.

Song, S., et al., 2020. Synthesis of Z-scheme multi-shelled ZnO/$AgVO_3$ spheres as photocatalysts for the degradation of ciprofloxacin and reduction of chromium (VI). J. Mater. Sci. 55, 4987–5007. https://doi.org/10.1007/s10853-019-04316-8.

Song, W., et al., 2006. Photochemical production or depletion of hydrogen peroxide controlled by different electron transfer pathways in methyl viologen intercalated clays. Journal of Photochemistry & Photobiology A Chemistry 183, 31–34. https://doi.org/10.1016/j.jphotochem.2006.02.016.

Sturini, M., et al., 2012. Photolytic and photocatalytic degradation of fluoroquinolones in untreated river water under natural sunlight. Appl. Catal. B Environ. 119, 32–39. https://doi.org/10.1016/j.apcatb.2012.02.008.

Su, W., et al., 2010. Synthesis and catalytic performances of a novel photocatalyst BiOF. Scripta Mater. 62, 345–348. https://doi.org/10.1016/j.scriptamat.2009.10.039.

Trojanowicz, M., 2020. Removal of persistent organic pollutants (POPs) from waters and wastewaters by the use of ionizing radiation. Sci. Total Environ., 134425 https://doi.org/10.1016/j.scitotenv.2019.134425.

Vila, M., et al., 2013. α-Bi_2O_3 microcrystals and microrods: thermal synthesis, structural and luminescence properties. J. Alloys Compd. 548, 188–193. https://doi.org/10.1016/j.jallcom.2012.08.133.

Wang, H., et al., 2020. Bifunctional copper modified graphitic carbon nitride catalysts for efficient tetracycline removal: synergy of adsorption and photocatalytic degradation. Chin. Chem. Lett. 31, 2789–2794. https://doi.org/10.1016/j.cclet.2020.07.043.

Wang, W., et al., 2007. xBiOI-(1−x) BiOCl as efficient visible-light-driven photocatalysts. Scripta Mater. 56, 669–672. https://doi.org/10.1016/j.scriptamat.2006.12.023.

Wang, W., et al., 2019. Enhanced photocatalytic degradation performance of organic contaminants by heterojunction photocatalyst $BiVO_4/TiO_2$/RGO and its compatibility on four different tetracycline antibiotics. Adv. Powder Technol. 30, 1882–1896. https://doi.org/10.1016/j.apt.2019.06.006.

Wang, Y., et al., 2017. Controllable synthesis of metastable γ-Bi_2O_3 architectures and optical properties. Mater. Sci. Semicond. Process. 64, 55–62. https://doi.org/10.1016/j.mssp.2017.03.016.

Wei, et al., 2019. Enhanced photocatalytic degradation performance of organic contaminants by heterojunction photocatalyst $BiVO_4/TiO_2$/RGO and its compatibility on four different tetracycline antibiotics. Adv. Powder Technol. 30, 1882–1896. https://doi.org/10.1016/j.apt.2019.06.006.

Wei, L., et al., 2017. Transformation of erythromycin during secondary effluent soil aquifer recharging: removal contribution and degradation path. J. Environ. Sci. 51, 173–180. https://doi.org/10.1016/j.jes.2016.08.004.

Wen, X.J., et al., 2020. Photocatalytic degradation of sulfamethazine using a direct Z-Scheme AgI/$Bi_4V_2O_{11}$ photocatalyst: mineralization activity, degradation pathways and promoted charge separation mechanism, 121508 J. Hazard Mater. 385, 1–121508. https://doi.org/10.1016/j.jhazmat.2019.121508, 12.

Wu, C., et al., 2011. Hydrothermal synthesis and characterization of Bi_2O_3 nanowires. Mater. Lett. 65, 1134–1136. https://doi.org/10.1016/j.matlet.2011.01.021.

Wu, G., Xing, W., 2018. Fabrication of ternary visible-light-driven semiconductor photocatalyst and its effective photocatalytic performance. Mater. Technol. 34, 292–300. https://doi.org/10.1080/10667857.2018.1553267.

Wu, K., et al., 2020. Z-scheme BiOCl/Bi-Bi_2O_3 heterojunction with oxygen vacancy for excellent degradation performance of antibiotics and dyes. J. Mater. Sci. 55, 4017–4029. https://doi.org/10.1007/s10853-019-04300-2.

Xia, X., et al., 2020. Review study on sulfate-radical-based advanced oxidation processes for domestic/industrial wastewater treatment: degradation, efficiency, and mechanism. Frontiers in Chemistry 8, 592056. https://doi.org/10.3389/fchem.2020.592056.

Xiang, Z., et al., 2016. BiOI/$BiVO_4$ p-n heterojunction with enhanced photocatalytic activity under visible-light irradiation. J. Ind. Eng. Chem. 40, 83–92. https://doi.org/10.1016/j.jiec.2016.06.009.

Xie, J., et al., 2012. Template-free synthesis of hierarchical constructed flower-like δ-Bi_2O_3 microspheres with photocatalytic performance. Micro & Nano Lett. 7, 651–653. https://doi.org/10.1049/mnl.2012.0201.

Xu, Y., et al., 2019. Enhanced long-wavelength light utilization with polyani-line/bismuth-rich bismuth oxyhalide composite towards photocatalytic degradation of antibiotics. J. Colloid Interface Sci. 537, 101–111. https://doi.org/10.1016/j.jcis.2018.10.109.

Yan, Y., et al., 2014. Template-free fabrication of α- and β-Bi_2O_3 hollow spheres and their visible light photocatalytic activity for water purification. J. Alloys Compd. 605, 102–108. https://doi.org/10.1016/j.jallcom.2014.03.111.

Yang, Y., et al., 2018. BiOX (X= Cl, Br, I) photocatalytic nanomaterials: applications for fuels and environmental management. Adv. Colloid Interface Sci. 254, 76–93. https://doi.org/10.1016/j.cis.2018.03.004.

Ye, L., et al., 2014. Recent advances in BiOX (X= Cl, Br and I) photocatalysts: synthesis, modification, facet effects and mechanisms. Environ. Sci.: Nano 1, 90–112. https://doi.org/10.1039/c3en00098b.

Yi, H., et al., 2018. Advanced photocatalytic Fenton-like process over biomimetic hemin-Bi_2WO_6 with enhanced pH. Journal of the Taiwan Institute of Chemical Engineers 93, 184–192. https://doi.org/10.1016/j.jtice.2018.06.037.

Yin, S., et al., 2015. Recent progress in g-C_3N_4 based low-cost photocatalytic system: activity enhancement and emerging applications. Catal. Sci. Technol 5, 5048–5061. https://doi.org/10.1039/C5CY00938C.

Yu, J., et al., 2005. Hydrothermal preparation and visible-light photocatalytic activity of Bi_2WO_6 powders. J. Solid State Chem. 178, 1968–1972. https://doi.org/10.1016/j.jssc.2005.04.003.

Yu, P., et al., 2020. Inactivation and change of tetracycline-resistant Escherichia coli in secondary effluent by visible light-driven photocatalytic process using Ag/AgBr/g-C_3N_4. Sci. Total Environ. 705, 135639. https://doi.org/10.1016/j.scitotenv.2019.135639.

Zhao, H., et al., 2019. g-C_3N_4 surface-decorated $Bi_2O_2CO_3$ for improved photocatalytic performance: theoretical calculation and photodegradation of antibiotics in actual water matrix. Chem. Eng. J. 366, 468–479. https://doi.org/10.1016/j.cej.2019.02.088.

Zhang, G., et al., 2013. Rapid microwave-assisted synthesis of Bi_2O_3 tubes and photocatalytic properties for antibiotics. Micro & Nano Lett. 8, 177–180. https://doi.org/10.1049/mnl.2013.0074.

Zhang, L., et al., 2015. Photoreduction of CO_2 on BiOCl nanoplates with the assistance of photoinduced oxygen vacancies. Nano Research 8, 821–831. https://doi.org/10.1007/s12274-014-0564-2.

Zhang, L., et al., 2018. Development of Bismuth Oxide-Based Materials for Iodide Capture and Photocatalysis. Kent State University. http://orcid.org/0000-0002-5613-5292.

Zhang, M., et al., 2019. Ultrathin oxygen-vacancy abundant WO_3 decorated monolayer Bi_2WO_6 nanosheet: a 2D/2D heterojunction for the degradation of Ciprofloxacin under visible and NIR light irradiation. J. Colloid Interface Sci. 556, 557–567. https://doi.org/10.1016/j.jcis.2019.08.101.

Zhang, Q., et al., 2015. Comprehensive evaluation of antibiotics emission and fate in the river basins of China: source analysis, multimedia modeling, and linkage to bacterial resistance. Environ. Sci. Technol. 49, 6772–6782. https://doi.org/10.1021/acs.est.5b00729.

Zhang, X., et al., 2015. Degradation of ciprofloxacin in aqueous bismuth oxybromide (BiOBr) suspensions under visible light irradiation: a direct hole oxidation pathway. Chem. Eng. J. 274, 290–297. https://doi.org/10.1016/j.cej.2015.03.077.

Zhang, L., et al., 2010. Effective photocatalytic disinfection of E. coli K-12 using AgBr−Ag−Bi_2WO_6 nanojunction system irradiated by visible light: the role of diffusing hydroxyl radicals. Environ. Sci. Technol. 44, 1392–1398. https://doi.org/10.1021/es903087w.

Zhao, G., et al., 2021. Construction of a visible-light-driven magnetic dual Z-scheme Bi-VO_4/g-C_3N_4/$NiFe_2O_4$ photocatalyst for effective removal of ofloxacin: mechanisms and degradation pathway. Chem. Eng. J. 405, 126704. https://doi.org/10.1016/j.cej.2020.126704.

Zhao, M., et al., 2004. Bi_2O_3 nanosquaresheets grown on Si substrate. Appl. Phys. A 78, 291–293. https://doi.org/10.1007/s00339-003-2345-8.

Zhao, Y., et al., 2018. Degradation and removal of Ceftriaxone sodium in aquatic environment with Bi_2WO_6/g-C_3N_4 photocatalyst. J. Colloid Interface Sci. 523, 7–17. https://doi.org/10.1016/j.jcis.2018.03.078.

Zheng, H., et al., 2018. $KBiO_3$ as an effective visible-light-driven photocatalyst: degradation mechanism for different organic pollutants. Chemphotochem 2, 442–449. https://doi.org/10.1002/cptc.201700211.

Zhou, L., et al., 2013. Degradation of organic pollutants in wastewater by bicar-bonate-activated hydrogen peroxide with a supported cobalt catalyst. Environ. Sci. Technol. 47, 3833–3839. https://doi.org/10.1021/es400101f.

Zhou, L., et al., 2020. 0D/2D plasmonic Cu_2-xS/g-C_3N_4 nanosheets harnessing UV-vis-NIR broad spectrum for photocatalytic degradation of antibiotic pollutant. Appl. Catal. B Environ. 263, 118326. https://doi.org/10.1016/j.apcatb.2019.118326.

Zhou, Z., et al., 2020. Mechanistic insights for efficient inactivation of antibiotic resistance genes: a synergistic interfacial adsorption and photocatalytic-oxidation process. Sci. Bull. 65 (24), 2107–2119. https://doi.org/10.1016/j.scib.2020.07.015.

Zhu, F., et al., 2020. Enhanced visible light photocatalytic performance with metal-doped Bi_2WO_6 for typical fluoroquinolones degradation: efficiencies, pathways and mechanisms. Chemosphere 252, 126577. https://doi.org/10.1016/j.chemosphere.2020.126577.

Zhu, X., et al., 2013. Photocatalytic degradation of tetracycline in aqueous solution by nanosized TiO_2. Chemosphere 92, 925–932. https://doi.org/10.1016/j.chemosphere.2013.02.066.

Zhu, Y., et al., 2017. Enhanced photocatalytic activity of magnetic core-shell Fe_3O_4@Bi_2O_3-RGO heterojunctions for quinolone antibiotics degradation under visible light. J. Mater. Sci. Mater. Electron. 28, 8519–8528. https://doi.org/10.1007/s10854-017-6574-6.

Zhu, Z., et al., 2017. A novel p-n heterojunction of $BiVO_4$/TiO_2/GO composite for enhanced visible-light-driven photocatalytic activity. Mater. Lett. 209, 379–383. https://doi.org/10.1016/j.matlet.2017.08.045.

Zhu, Z., et al., 2020. Synthesis of novel ternary photocatalyst Ag_3PO_4/Bi_2WO_6/multi-walled carbon nanotubes and its enhanced visible-light photoactivity for photodegradation of norfloxacin. J. Nanosci. Nanotechnol. 20, 2247–2258. https://doi.org/10.1166/jnn.2020.17368.

Zhuang, X., et al., 2020. Enhanced sulfamerazine removal via adsorption-photocatalysis using Bi_2O_3-TiO_2/PAC ternary nanoparticles. Water 12, 2273. https://doi.org/10.3390/w12082273.

Zuo, X., et al., 2019. Enhanced multiferroicity and narrow band gap in B-site Co-doped Aurivillius $Bi_5FeTi_3O_{15}$. Ceram. Int. 45, 137–143. https://doi.org/10.1016/j.ceramint.2018.09.144.